# Persistent immune stimulation exacerbates genetically-driven myeloproliferative disorders via stroma remodelling

Claudio Tripodo[1*], Alessia Burocchi[2*], Pier Paolo Piccaluga[3], Claudia Chiodoni[2], Paola Portararo[2], Barbara Cappetti[2], Laura Botti[2], Alessandro Gulino[1], Alessandro Isidori[5], Arcangelo Liso[6], Giuseppe Visani[5], Maria Paola Martelli[7], Brunangelo Falini[7], Pier Paolo Pandolfi[8], Mario P. Colombo[2§] and Sabina Sangaletti[2§]

1. Tumor Immunology Unit, Human Pathology Section, Department of Health Science, Palermo University School of Medicine, Palermo, Italy.
2. Department of Experimental Oncology and Molecular Medicine, Fondazione IRCCS Istituto Nazionale Tumori, Milan, Italy.
3. Department of Experimental, Diagnostic, and Experimental Medicine, S. Orsola-Malpighi Hospital, Bologna University School of Medicine, Bologna, Italy.
4. Biomedical Department of Internal and Specialized Medicine, Palermo University school of Medicine, Palermo, Italy.
5. Hematology and Hematopoietic Stem Cell Transplant Center, AORMN, Pesaro, Italy
6. Department of Hematology, University of Foggia, Foggia, Italy
7. University of Perugia, Perugia, Italy.
8. Cancer Research Institute and Departments of Medicine and Pathology, Beth Israel Deaconess Medical Center, Harvard Medical School, Boston, USA.

Conflict of interest disclosure statement: The Authors have no conflict of interest to declare.

Contact information: Correspondance to: sabina.sangaletti@istitutotumori.mi.it or mariopaolo.colombo@istitutotumori.mi.it

Additional footnotes *Co-first and §co-senior authorship

Running title: NET-related immune stimulation promotes myeloproliferation

Abstract count: 211 words

Main text count: 4918 words

**Abstract**

Systemic immune stimulation has been associated with an increased risk of myeloid malignancies, but the pathogenic link is unknown. We demonstrate that, in animal models, experimental systemic immune activation alters the bone marrow stromal microenvironment disarranging extracellular matrix (ECM) microarchitecture, with downregulation of SPARC and collagen-I and induction of complement activation. These changes are accompanied by a decrease in Treg frequency and by an increase in activated effector T cells. Under these conditions, hematopoietic precursors harboring *nucleophosmin-1* (*NPM1*) mutation generate myeloid cells unfit for normal hematopoiesis but prone to immunogenic death, leading to neutrophil extracellular trap (NETs) formation. NETs foster the progression of the indolent *NPM1*-driven myeloproliferation toward an exacerbated and proliferative dysplastic phenotype. Enrichment in NET structures was found in the BM of patients with autoimmune disorders and in *NPM1*-mutated AML patients. Genes involved in NET formation in the experimental model were used to design a NET-related inflammatory gene signature to be tested on human myeloid malignancies. This signature identified two AML subsets with different genetic complexity and different enrichment in *NPM1* mutation, and predicted the response to immunomodulatory drugs. Our data indicate that stromal/ECM changes and priming of BM NETosis by systemic inflammatory conditions can complement genetic and/or epigenetic events towards the development and progression of a myeloid malignancy.

## Introduction

Alterations in the bone marrow (BM) osteoblastic and vascular niches that nurture hematopoietic stem cells (HSCs) are associated with the outgrowth of myeloid cells within a biased leukemic niche (1,2). Such alterations encompass the adaptation of specific mesenchymal cell populations and the disruption of normal gradients in structural and secreted proteins, including matricellular proteins, cytokines, and chemokines (3). A key regulator of BM stromal changes is the secreted protein acidic and rich in cysteine (SPARC) (4), a matricellular protein which up-and down-regulation has been associated with hematological neoplasms (2,5).

Along with remodeling of the BM mesenchymal architecture, myeloid clone expansion changes the cytokine profile of the hematopoietic milieu. Increased levels of pro-inflammatory cytokines including TNF, IL-6, and IL-8 have been reported in patients with myeloproliferative neoplasms, myelodysplastic syndromes, and myeloid leukemia with an unfavorable predicted disease course (6,7). The induction of an inflammatory state in the myelopoietic parenchyma is mutually linked with the status of the stromal architecture. A defective ECM organization resulting from SPARC deficiency favors the over-activation of myeloid cells (8) and granulocyte immunogenic death via the formation of neutrophil extracellular traps (NETs) (5). NETotic death is characterized by the expression of interferon response related transcriptional programs associated with the induction of inflammation and exacerbation of autoimmune disease, in which NETs contribute as sources of autoantigens and co-stimulatory signals (9-13). A link has been demonstrated between dysregulated immune stimulation and the occurrence of myeloid malignancies. Large-scale epidemiological studies have shown that the history of chronic autoinflammatory or autoimmune diseases is correlated with increased incidence of myelodysplastic syndromes (MDS) or acute myeloid leukemia (AML) (14); however, the role of systemic immune activation in the pathobiology of myeloid malignancies remains unknown. The highest risk of development of MDS and AML has been reported in patients with autoimmune diseases in which NETs have a recognized pathogenic role, e.g., systemic lupus erythematosus and antineutrophil cytoplasmic antibody (ANCA)-related vasculitis (9,15).

In this study, we investigated whether a persistent immune stimulation can change the BM stromal microenvironment and affect hematopoietic precursor proliferation. We identified a novel regulation of myeloid cell expansion involving the crosstalk between the immune cells and stromal components of the BM microenvironment. Such crosstalk is proposed to be relevant in explaining the link between systemic immune activation and myeloid neoplasms.

## Material and Methods

*Mice*

hMPR8-NPMc$^+$ transgenic mice (B6. Tg<hMRP8-NPMc>Ptprc<b>tg/J), hereafter referred as *NPMc*, were obtained by backcrossing (C57BL/6J × CBA) F1-hMRP8-NPMc mice to C57BL/6 (B6. Ptprc<b>). The BM of *Trif*$^{-/-}$ mice was kindly provided by Dr. Garlanda (Humanitas Clinical and Research Center). All experiments involving animals described in this study were approved by the Ministry of Health (authorization number 10/11). The protocol describing the immunization of WT and NPMc mice with NET-loaded DCs is described in Supplemental Data.

*Human and murine BM histology, immunohistochemistry, and immunofluorescence*

Histological, histochemical, and immunofluorescence analyses of murine and human BM samples were performed as previously described (Tripodo et al., 2012) (Sangaletti et al., 2014a) and detailed in the Supplemental Data. For in situ histopathological analyses of human BM specimens, the BM biopsies from 12 patients with autoimmunity-associated peripheral cytopenias were selected from the archives of the Department of Hematology, University of Foggia and the Department of Health Sciences, University of Palermo. Patient characteristics are listed in Supplementary Table 1.

*BM and spleen FACS analysis of hematopoietic precursors*

Briefly marrow and spleen cell suspensions were stained with a pool of antibodies for Lin positive markers, including CD3, CD11b, CD45R, Ly6G, CD4, CD8, and Ter-119, and stem cell and progenitor cell markers, including CD117 (c-Kit), CD34, and CD16/CD32. Progenitors were identified according to their expression of CD34 and CD16/CD32 within the gate of Lin$^-$CD117$^+$ cells. BM, spleens and PBL samples were also evaluated for granulocyte enrichment by staining cell suspensions with mAbs against CD11b, Ly6G, and CD45, followed by FACS analysis. All antibodies were purchased from eBioscience. Samples were acquired on an LSR II (BD Biosciences).

*Immunization of WT and NPMc pre-leukemic mice with NET-loaded DCs*

Inflammatory PMNs (IFNγ/TNF-treated), prone to dye of NETosis, were obtained from agar plugs subcutaneously injected into C57BL/6 mice, as previously described (9). In particular, PMN were seeded onto coated tissue culture dishes in IMDM 2% FCS, allowed to adhere for 30 minutes and added with mDCs (1:1; PMN:DC) for 16h. During this period NETs are induced and transfer their component to mDCs (9). DCs were isolated from the co-culture via positive selection, counted and

injected i.p (2.5-5x$10^6$ cells, once a week for a total of 6 injections) into naïve mice. Three months after the last immunization, mice underwent a boosting immunization. Autoimmunity was evaluated starting 1 month after the boost by measuring the titer of ANCA and ds-DNA auto-antibodies using specific ELISA kits (MPO-ANCA IgG, ELISA Kit from Cusabio and mouse anti-dsDNA antibody ELISA Kit from Alpha Diagnostic International)

*Qualitative and quantitative evaluation of NET formation.*

For *ex-vivo* isolated neutrophils, spontaneous NETosis was evaluated by seeding BM-derived PMNs onto poly-D-lysine coated glasses in 2% FCS-IMDM in presence or absence of PMA (16). To quantify NETosis and to distinguish NETosis from apoptosis, the cell-impermeable DNA dye Sytox green, was added to PMNs such to measure the size of the released nuclear contents from micrographs using the software-assisted technique, according to Metzler and coworkers (17). To assess NET formation *in vivo* in murine and human BM-biopsies, confocal microscopy analysis was performed by staining with mAbs to murine or human-MPO (from Millipore and Novocastra, respectively) and anti-Histone H3 (citrulline R2+R8+R17, from abcam), followed by staining with Alexa Fluor 546-conjugated goat anti-rabbit or goat anti-mouse secondary antibodies (Invitrogen Molecular Probes). Nuclei were counterstained with Draq5 or Dapi. To evaluate NPMc re-localization onto the NET threads, PMA-induced NETs (splenic WT and NPMc PMN treated 16h with PMA) were sequentially stained with mAb to NPM (18) and MPO (Millipore) or PR3 (Millipore). The NET-DNA was counterstained with Draq5.

*In vitro cultures of Lin$^-$c-Kit$^+$ hematopoietic cells*

*Lin$^-$c-Kit$^+$* cells were FACS-sorted from the BM of NPMc or control mice (BD, FACSAria), stained with Carboxyfluorescein succinimidyl ester (CFSE) and added to PMNs undergoing NETosis (inflammatory PMNs from agar plugs (9) or PMA-treated PMNs). The co-culture was performed in StemSpan H3000 medium (Stem Cell Technologies), without adding any other supplement. After 72h of cu-culture, cells are harvested and the c-Kit$^+$ cell fraction, which comprised c-Kit$^+$Sca$^+$GR-1$^-$ early progenitors, c-Kit$^+$Sca$^-$GR-1$^-$ committed precursors (mostly GMP), and c-Kit$^+$Sca$^-$GR-1$^+$ myeloblasts, was analyzed for proliferation. Proliferation was read out by measuring dilution of the CFSE dye (19).

*Gene expression profile analysis*

Gene expression profile (GEP) analysis was performed in a panel of primary hematopoietic malignancies, including AML (AN=100), chronic myelogenous leukemia (CML, N=50), MDS

(N=50) and in a panel of healthy bone marrow samples (N=30), which were randomly selected among those included in a large multicentric GEP study available on GEO database (GSE13159)(20,21). We also analyzed 461 AML cases for which gene expression data as well as information on the *NPM1* status (mutated vs. wild type) were available (GEO Access: GSE6891) (22) (23) and 15 AML cases included in a phase II clinical trial testing the combination of lenalidomide and cytarabine (Len-Ara) and for which our group previously generated GEP (24). Each case was assigned to either group 1 or 2 based on the expression of the NET-related inflammatory signature. A detailed description of the analysis performed is provided in Supplemental Data.

**Results**

*Systemic autoimmunity induces modifications in the bone marrow stromal and immune cell compartments.*

To investigate how systemic autoimmunity could affects BM stroma remodelling, naïve C57BL/6 mice were repeatedly immunized by intraperitoneal injections of myeloid dendritic cells (mDCs) loaded with NET components (Figure 1A and Supplemental Data). As previously shown (9), immunized mice developed serum autoantibodies and ANCA-associated autoimmune vasculitis in the kidney and lung parenchyma (Figure 1B and Supplementary Figure 1A-B). Compared to naïve mice, the BM of immunized mice showed a significant decrease in the levels of type-I collagen and SPARC, as assessed by semi-quantitative PCR (Figure 1C), immunohistochemistry (Figure 1D) and *in situ* immunofluorescence (Supplementary Figure 1C). The decrease in type-I collagen and SPARC was particularly evident in CD29+ stromal cells lining the osteoblastic (OB) niche, which is enriched in c-Kit$^+$ precursors (Figure 1F). Moreover, stromal and endothelial BM cells showed increased C1q expression which was associated with C5a (Figure 1G-I), suggesting activation of the complement cascade. Finally, a trend in the induction of P-selectin expression was also observed in the BM of immunized mice (Supplementary Figure 1D-F).

Foxp3$^+$ Treg cells are typically either depleted or skewed towards inflammatory Th1 or Th17 cells under autoimmune conditions (25). In the BM of naïve mice, nearly 30% of CD4$^+$ T cells were Foxp3$^+$ Treg cells, a frequency much higher than that of the other lymphoid organs, where Treg cells accounted for 5-15% of total CD4$^+$ T cells (Supplementary Figure 1G-H). In contrast, in the BM of immunized mice the frequency of Treg cells was significantly reduced (Figure 2A). Also reduced in this subset was the expression of OX40(26), a marker of activation (Figure 2A). On the contrary, the expression of CD25 and OX40 on Teff cells was increased (Figure 2B) together with their production of IFNγ and TNF (Figure 2C-D). In immunized mice, TNF and IFNγ were also induced in CD45$^+$ cells other than T lymphocytes (Figure 2E).

To test the existence of a link between the TNF- and IFNγ-rich inflammatory milieu and stromal ECM modifications, BM-MSCs were isolated from the BM of naïve mice and stimulated 24 h with IFNγ, TNF or both. Semi-quantitative PCR analysis showed that these stimuli, mostly when in combination, significantly decrease the expression of *col1a1* and *Sparc* in BM-MSCs (Figure 2F-G).

Collectively, these results show that systemic immune activation modifies the BM stromal microenvironment and changes the immune cell composition from immune-regulatory to pro-inflammatory.

*NET formation in a pro-inflammatory BM microenvironment promotes HSC proliferation via IL-6, SCF, and NF-kB activation.*

TNF, IFNγ (9) and complement factors (27) are major drivers of NET formation. In a context of defective ECM molecules (collagens and SPARC) their NET-inducing capacity increases because of the lack of inhibitory signals that are provided by collagens (5). Therefore we investigated whether induction of systemic autoimmunity affected NET formation by BM cells. Immunized mice showed increased NET formation, as assessed *ex vivo* by measuring the capacity of BM-derived polymorphonuclear leukocytes (PMNs) to undergo spontaneous NETosis (Figure 2H-I) as well as *in situ* by immunoflourescence (Figure 2J) and confocal microscopy (Figure 2K).

We then investigated the capacity of NETs to affect the proliferation of BM hematopoietic cells. $Lin^{-}c\text{-}Kit^{+}$ (LK) hematopoietic cells were sorted from the BM, stained with carboxyfluorescein succinimidyl ester (CFSE) and co-cultured with NETs in conditions enabling HSC maintenance and differentiation towards myeloid lineages. As a source of NETs, we used PMNs isolated from *in vivo* inflammatory foci that undergo spontaneous NETosis dependent on TNF and IFNγ priming (9). In some experiments, PMA-treated NETotic PMNs were used as positive controls (28). Starting from 72h of co-culture, NETotic, but not apoptotic, necrotic, or naïve PMNs, significantly enhanced the proliferation of $c\text{-}Kit^{+}$ BM cells (Supplementary Figure 2A). An in depth analysis showed that NET specifically enhanced the proliferation of c-Kit+Sca+GR-1- early progenitors (LSK), c-Kit+Sca-GR-1- (LK) committed precursors (mostly GMP), and c-Kit+Sca-GR-1+ myeloblasts (Figure 2L, representative gating strategy in Supplementary Figure 2B). Moreover, NETs sustained the expression of Sca-1 in $c\text{-}Kit^{+}Sca^{+}Gr\text{-}1^{-}$ early progenitor cells, which is crucial for HSC self-renewal and proliferation (Figure 2M).

Investigating the mechanism involved in NET-induced proliferation of c-Kit+ cells we first excluded the involvement of TLRs as sensor of the NET DNA-backbone (Supplementary Figure 2C-D). Considering that the proliferation of $c\text{-}Kit^{+}$ cells induced by NETs was diminished by the interposition of a transwell membrane (Supplementary Figure 2E-F), we evaluated the role of soluble mediators. Stem cell factor (SCF) and IL-6 are known to promote hematopoietic cell renewal and clonogenic capacity through NF-kB (29). MAbs blocking either the IL-6 receptor (15A7) or c-Kit (ACK2) strongly inhibited NET-induced proliferation of $c\text{-}Kit^{+}$ hematopoietic cells, an effect magnified by the simultaneous blockade of both receptors (Figure 2N). Pharmacological inhibition of NF-kB had a comparable effect (Figure 2O), being NF-kB the main transducer of IL-6R on hematopoietic precursors (30). These data indicate that NET inflammatory pressure exerted on $c\text{-}Kit^{+}$ hematopoietic cells through IL-6 and SCF release confers a proliferative advantage to

hematopoietic precursors.

*NET-associated immune stimulation exacerbates NPM1 mutation-driven myeloproliferation in vivo.* We then investigated whether NET-induced stimulation of hematopoietic precursors could impact on the proliferation of myeloid cells under myeloproliferative conditions *in vivo*. *NPMc* transgenic mice carry the human mutated *NPMc* under a myeloid-specific promoter and are prone to develop an indolent myeloproliferation, in which mature myeloid cells expand without progressing towards myelodysplasia or leukemia (31). Induction of systemic autoimmunity in *NPMc* transgenic mice elicited modifications in the BM microenvironment that mirrored those observed in immunized WT mice (Supplementary Figure 3 and 4) and included *in situ* formation of NETs (Supplementary Figure 5A).

Compared to naïve *NPMc* mice, a significantly higher percentage of immunized *NPMc* mice developed a myeloproliferative disorder at approximately 12 months of age (60% vs 25%, $p<0.05$). In these mice, BM histopathology revealed an exacerbated myelodysplastic/myeloproliferative phenotype with a left-shift of myelopoiesis, clustering of atypical myeloid precursors, dysmegakaryopoiesis, and signs of intravascular hematopoiesis (Figure 3A). Paralleling the exacerbated myeloproliferation the BM of immunized NPMc mice showed a significant difference in the density of BM erythroid colonies highlighted by TER-119 immunostaining (Figure 3B).
Consistently, the frequency of cytoplasmic NPM-expressing elements and of proliferating Ki-67-expressing myeloid elements in the BM of immunized *NPMc* mice was significantly higher as compared with naïve *NPMc* controls (Figure 3C-E). Moreover, BM smears of immunized *NPMc* mice showed an increase in immature forms of myeloid cells with atypical morphology (Figure 3F, red arrows), a concomitant decrease in segmented mature granulocytes (black arrows), and an increase in lymphoid elements (green arrows). Flow cytometry analysis of the BM showed a significant expansion in the fraction of hematopoetic precursors (LK and LSK) and committed progenitors (GMP, MEP), megakaryocytes and megakaryocyte precursors in immunized *NPMc* mice. Conversely, the total number of B220+ B cells decreased (Figure 3G; Supplementary Figure 5B for representative gating strategy).
Dysplastic features were also found in megakaryocytic and granulocytic cells within extramedullary splenic hematopoietic foci, which were expanded in immunized *NPMc* mice (Supplementary Figure 6A). Indeed, the frequency of cytoplasmic NPM-expressing elements and of proliferating Ki-67-expressing myeloid elements was increased in the spleen of immunized *NPMc* mice (Supplementary Figure 6B-E). Flow cytometry analysis of spleen myeloid populations showed a significant expansion in the amount of LK cells and of granulocyte-monocyte progenitor (GMP) in

immunized *NPMc* mice (Supplementary Figure 6F-I). Finally, c-Kit$^+$ blasts had a higher frequency in the blood of immunized *NPMc* mice, a finding corroborated by the enrichment in morphologically-immature circulating myeloid cells (Figure 3 H-I).

To provide an alternative approach testing the impact of persistent immune stimulation on the take of an established acute leukemia, we adopted the C1498 murine leukemia model (32). C57BL/6 mice were either immunized or not with DCs loaded with NET components and one month after the last immunization they were injected intra-bone with $2x10^5$ GFP-labeled C1498 cells. Twenty-eight days after cell injection, mice were sacrificed and evaluated for the presence of C1498 in the BM by FACS. Immunization significantly promoted the leukemic cell take in the BM with the increased fraction of C1498 cells inversely correlating with that of B220+ resident cells, which were outcompeted (Supplementary Figure 7). These results indicate that systemic and persistent immune activation can exacerbate the phenotype of a genetically driven myeloproliferative spur.

*NPMc mutation affects the NETosis of PMN and NET-induced proliferation of c-Kit+ cells*

Considering the data obtained in immunized *NPMc* mice, we hypothesized that NETs could confer a stronger proliferative advantage to hematopoietic precursors of *NPMc* rather than WT genotype. The presence of the *NPMc* mutation did not confer an intrinsic proliferative advantage to c-Kit$^+$ cells in response to NET stimulation (Figure 4A). In line, LSK cells from *NPMc* and WT mice co-cultured with NETs in the absence of any growth factor (i.e., SCF or IL-3) were equally able to survive in culture and to reconstitute lethally irradiated mice (Figure 4B).

We then investigated whether BM myeloid cells from *NPMc* and WT mice were differently prone to NET formation. BM PMNs from *NPMc* and WT mice were seeded onto poly-D-Lysine-coated slides and treated with IFNγ plus C5a or PMA. In both conditions, BM PMNs from *NPMc* mice showed a significantly increased NET formation in response to inflammatory stimuli (Figure 4D-E). Moreover, NETs from *NPMc* mice were more efficient in enhancing proliferation of c-Kit$^+$ cells (Figure 4F).

As NPM may act as an alarmin and contribute to systemic inflammation, e.g., during sepsis (33), we hypothesized that the *NPMc* mutation, which causes cytoplasmic NPM localization (34), could be responsible for NPM reallocation onto NETs, thereby influencing its availability as a NET-associated alarmin. IHC analyses performed on BM sections showed that NPM, which is almost absent in mature BM-PMNs of WT mice, is detectable in the cytoplasm of BM PMNs from *NPMc* mice (Figure 4G). In these mice, immunofluorescence on BM sections using an anti-NPM Ab detecting both normal and mutated NPM, also highlighted NET threads (Figure 4H). Moreover,

at confocal microscopy, *ex-vivo* NET from *NPMc* mice displayed NPM relocalized onto the NET DNA threads (Figure 4I), where it associated with classical NET cytoplasmic proteins, such as MPO (Figure 4 J).

To test the ability of extracellular NPM to act as an alarmin for hematopoietic cells, LK cells were cultured in the presence of recombinant human and mouse NPM. As a result, proliferation of c-Kit$^+$ cells exposed to extracellular NPM was significantly enhanced in a dose-dependent manner and this effect could be inhibited by NF-kB blockade (Figure 4K-L). Recombinant NPM mimicked TNF and IFNγ inflammatory stimuli in down-modulating the expression of ECM molecules in BM-MSCs (Figure 4M), a condition that promotes NET formation, delineating a self-sustaining inflammatory loop in AML carrying *NPM1* mutation.

*In situ NET formation can be identified in patients with systemic autoimmunity and in AML patients with NPM1 mutation.*

In order to establish the translational significance of findings in experimental models, we performed studies in patients with systemic autoimmunity and in myeloid malignancies. Analysis of the BM of patients with unexplained peripheral cytopenias and signs of systemic autoimmunity (AUC) (Supplementary Table 1) showed mild alteration in granulocytic and megakaryocytic differentiation that did not configure impaired hematopoiesis or frank myelodysplasia when compared to normal controls (not shown). No significant differences were found in the overall amounts of BM-infiltrating T cells; however, a trend towards the reduction of Foxp3$^+$ Treg cells was observed in the BM of patients with autoimmune disorders (Figure 5A-B). Most importantly, in these same patients, NETs were identified *in situ* by staining for MPO and DAPI (Figure 5C). In patients with circulating autoantibodies (Supplementary Table 1), NET extracellular MPO threads were associated with C1q deposition (Figure 5D).

We then investigated the presence of NETs in the BM of AML patients carrying mutations in the *NPM1* gene. Immunofluorescence analysis for the chromatin marker Histone-H3 and either MPO or NPM was performed on twenty cases of AML with mutated (N=10) or WT (N=10) *NPM1*. We found that, in human AML cases, NETs were detected as Histone-H3$^+$ threads associated with MPO in cases in which MPO expression was preserved (Figure 5E). As shown in transgenic *NPMc* mice, in the BM of patients with *NPM1*-mutated AML NET figures could be identified as characterized by the peculiar NPM localization onto the DNA thread marked by Histone-H3 (Figure 5E). Quantification of NET figures as highlighted by Histone H3 and NPM or MPO on 5 high-power magnification microscopic fields, revealed that a higher frequency of NET figures could be identified in *NPM1* mutated cases (Figure 5F and Supplementary Table 2). These data suggest that

formation of NETs in the BM observed in experimental systemic autoimmunity can be also observed in spontaneously occurring human autoimmune pathologies and occurs within the BM environment of AML with mutated *NPM1*.

*A NET-related inflammatory gene signature discriminates myeloid leukemia subsets*

We then asked whether the inflammatory profile related with NETosis could be differently enriched at the transcriptional level in human myeloid malignancies.

To this end, we designed an *ad hoc* gene signature representative of the pathways activated in the BM upon immunization and implicated in NET induction (Supplementary table 3) (5). The signature, thereafter referred to as NET-related inflammatory signature, was analyzed in a large panel of primary hematopoietic malignancies, including AML (N = 100), chronic myelogenous leukemia (CML, N = 50), MDS (N = 50), and in healthy BM samples (N = 30), obtained from a large multicentric GEP study (See the Supplementary information). Unsupervised hierarchical clustering based on the expression of the NET-related inflammatory signature separated AML samples from CML, MDS, and healthy BM samples (Supplementary Figure 8A). When a supervised approach was used to identify, within the NET-related inflammatory signature, the most suitable genes to differentiate the various diseases (ANOVA, $p < 0.05$, fold change > 2), AML was again separated from the other samples (Supplementary Figure 8B).

Considering the variability in the NET-related inflammatory gene expression profiles in AML we investigated the AML cases in depth in order to understand the contribution of inflammation-related genes in this pathological setting. We identified 20 genes (corresponding to 27 probe sets) belonging to the NET-related inflammatory signature that were differentially expressed in AML *vs* healthy BM samples (t-test, $p<0.05$, fold change >2, Supplementary Table 4). Based on the expression of these genes, AML cases could be divided into two clusters: Cluster 1 and Cluster 2 (Supplementary Figure 8C). A supervised analysis (t-test, $p<0.05$; multiple testing correction: Bonferroni family wise error rate) was then performed to identify differentially expressed genes in Cluster 1 and Cluster 2. We identified 592 probe sets that enabled efficient discrimination between the two clusters (Supplementary Table 5; Figure 6A). When studied by Gene Set Enrichment analysis (GSEA) the corresponding 440 genes turned out to be significantly associated, as expected, with inflammation and immune response programs as well as with other relevant cellular processes and pathways, including some related with signal transduction, hematopoietic and leukemic stemness and, most notably, NPM1 signaling (Supplementary Table 6; Figure 6B). This expression pattern was not found to be related to cytogenetic features in AML. Indeed, the two AML clusters comprised all different karyotypic groups (Supplementary Figure 8D). Furthermore, the 17 genes

(corresponding to 25 probe sets) belonging to the NET-related inflammatory signature, which were differentially modulated across the cytogenetic groups, as identified by supervised analysis (ANOVA, $p < 0.05$, fold change >2), were unable to clearly discriminate between AML cases with different karyotypic abnormalities (Supplementary Figure 8E-F).

We extended the supervised analysis to an independent panel of 461 AML cases for which gene expression data, information on *NPM1* mutational status, and clinical follow-up were available (GEO Access: GSE6891 (23)). Again, the identified NET-related inflammatory signature defined two AML clusters in which mutated and wild-type *NPM1* cases were significantly segregated (chi-square, $p < 0.001$; Figure 6C). Similar results were obtained by performing hierarchical clustering based on the expression of the 440 genes (Supplementary Table 5) discriminating the two AML clusters: *NPM1*-mutated and *NPM1*-wild type cases were significantly divided (chi-square, $p < 0.001$; Supplementary Figure 8G). This pattern was independent from karyotype, in particular cases with normal karyotype were homogeneously distributed in the two clusters (chi-square, p=0.19). Consistently, we found that differentially expressed genes in mutated versus wild-type *NPM1* cases were significantly enriched in the inflammatory response, IFNγ response, IL-6 signaling, and complement cascade programs at gene set enrichment analysis (Supplementary Table 7). Conversely, when gene expression profiles of cases presenting with somatic mutations affecting leukemia-associated genes other than NPM1 (*CEBPA, IDH1, IDH2, KRAS, NRAS*, and *FLT3*-ITD) were investigated, IDH1-mutated cases were found to display significant enrichment in genes belonging to the NET-related signature, even if only very few cases (N=3) among those of the analyzed panel had isolated *IDH1* mutations.

*The NET-related inflammatory gene signature predicts response to immunomodulatory drugs.*

To assess the potential clinical impact of NET-related inflammatory features, we applied our signature to a cohort of high-risk AML patients (N = 26; CR=14; noCR=12)) treated with the combination of chemotherapy and the immunomodulatory drug lenalidomide (24). The molecular signature associated with complete response (24) significantly overlapped with the NET-related inflammatory signature (chi-square, p=0.03), being also enriched in genes characteristic of NPM1 mutated AML. In the same cohort of patients, the NET-related inflammatory signature enabled subdivision of the AML cases into two groups with significantly different overall survival (median estimated survival 1 vs. 20 months, 95% confidence interval 0.140-6.88/1.86-45.11 months; $p < 0.001$; Figure 7A). A minimal signature consisting of three genes (Figure 7B) belonging to the NET-related inflammatory signature, namely *IRF7*, *C5AR1*, and *NF-KBIA*, were able to discriminate patients with a significantly better or worse outcome (p=0.03) (Figure 7C). Taken

together, these data showed that, though not associated with clinical outcome in a cohort of AML patients treated with conventional chemotherapy, the expression pattern of genes related with NETs was associated with the clinical response and survival of AML patients receiving the immunomodulatory agent lenalidomide.

**Discussion**

We showed that structural changes in the BM stroma are involved in shaping the myeloproliferative BM responses to systemic persisten immune stimulation. Immunization-induced autoimmunity was found to elicit downregulation of SPARC and type I collagen in the BM stroma as well as to promote local inflammatory conditions associated with T cell activation and NETosis. Within the BM, NET sustained the proliferation of hematopoietic precursors via the release of the hematopoietic cytokines SCF and IL-6 involving NF-kB.

The discovery of NET-induced expansion of hematopoietic precursors prompted us to investigate whether the transcriptional profiles of various human myeloid malignancies were differently enriched in a NET-related gene signature. We found that AML were divided into two main clusters according to the inflammatory imprint. The inflammatory cluster segregated according to NPM1 mutation-associated molecular programs. The NPM1 mutation is the most frequent genetic alteration identified in acute myeloid leukemia (AML) accounting for about 30% of all cases. This mutation defines a subgroup of AML with distinctive clinico-pathological features and it is also associated with a unique gene expression profile (18). The role of NPM1 mutation in leukemogenesis *in vivo* has not been fully elucidated. The low genetic complexity of NPM1-mutated AML suggests that this mutation requires additional stimuli, which might also be provided by the inflammatory microenvironment, to promote malignant clone progression (18).

In this context a large study involving 1540 patients has shown that the impact of NPM1 mutation on transformation become manifested only in presence of initiating mutations in epigenetic pathways, such as in DNMT3, TET2, IDH1/2 genes (35).

This makes no surprise that in the different transgenic (31) or conditional mouse model (36) (37), lacking addition mutations, a frank leukemia was rarely observed, although an indolent myeloproliferation, perturbed megakaryopoiesis or MPD have been reported. However, investigating whether an inflammatory BM environment was able to aggravate the indolent myeloproliferative phenotype of *NPMc* transgenic mice we found that features of dysplastic changes and increased extramedullary hematopoiesis were induced in *NPMc* immunized mice. The *NPMc* mutation cooperated with NET-mediated stimulation of c-Kit+ precursors according to the propensity of *NPMc* PMN to NETosis and because of the alarmin function of the NET-complexed cytoplasmic mutated NPM. This may explain, at least in part, why the NET-related inflammatory signature was found to be enriched in AML with mutated *NPM1*. Accordingly, the mutated NPM, although aberrantly translocated to the cytoplasm, conserves its functional domains, including the histone-binding domains (38) which may explain its affinity for histone-rich NET DNA threads and its related pro-alarmin function. This suggests that *NPMc*-bearing clones may benefit from the

presence of NET-triggering conditions, which may be irrelevant for clones with t(3,5) translocation (NPM1-MLF1) or loss of chromosome 5, which result in the loss of the DNA-binding domain or in the complete loss of NPM (39).

We discovered a novel role for NETs in stimulating hematopoietic precursor proliferation, also extending the influence of this form of myeloid cell death to hematopoiesis and related disorders. The identification of AML subgroups characterized by a NET-related inflammatory signature and BM NET induction claims for the investigation of immunomodulatory agent-containing treatments to be adopted in combination with conventional therapy in selected patients.

**Acknowledgments**

The authors thank Prof. Federica Sallusto (Institute for Research in Biomedicine, Università della Svizzera Italiana) and Prof. Niccolò Bolli (Fondazione IRCCS Istituto Tumori Milano) for critical reviewing of the manuscript. The authors also thank Professor Maurilio Ponzoni (Università Vita-Salute San Raffaele) and Professor Umberto Gianelli (Fondazione IRCCS Ca' Granda - Ospedale Maggiore Policlinico) for providing human tissue samples. The authors thank the Conventional and Confocal Microscopy Facility for confocal microscopy images acquisition, the Cell Sorting Facility for cell sorting and Mrs. Ester Grande for administrative assistance.

**Authorship Contributions**

SS, MPC and CT conceived the idea and designed the experiments. SS, AB, PP, LB, BC, CC, CG, CG, AI performed the experiments. SS, CT, CC, AB, AI, PPi analyzed the data. CT, PPi, PPa, GV, BF, AL, MPM contributed to data interpretation or provided key reagents. SS, CT and MPC wrote the manuscript.

**Grant support**

This work was supported by the Associazione Italiana per la Ricerca sul Cancro (My First AIRC Grant number 12810 to S. Sangaletti; Program Innovative Tools for Cancer Risk Assessment and Diagnosis, 5 per mille number 12162 to C. Tripodo and M.P. Colombo; Investigator Grant number 10137 to M.P. Colombo), and the Italian Ministry of Health (GR-2013-02355637 to S. Sangaletti).

**Disclosure of Conflicts of Interest**

The authors have no conflict of interest to declare.

references


1. Kode A, Manavalan JS, Mosialou I, Bhagat G, Rathinam CV, Luo N, et al. Leukaemogenesis induced by an activating beta-catenin mutation in osteoblasts. Nature 2014;506(7487):240-4.
2. Tripodo C, Di Bernardo A, Ternullo MP, Guarnotta C, Porcasi R, Ingrao S, et al. CD146(+) bone marrow osteoprogenitors increase in the advanced stages of primary myelofibrosis. Haematologica 2009;94(1):127-30.
3. Della Porta MG, Malcovati L, Boveri E, Travaglino E, Pietra D, Pascutto C, et al. Clinical relevance of bone marrow fibrosis and CD34-positive cell clusters in primary myelodysplastic syndromes. Journal of clinical oncology : official journal of the American Society of Clinical Oncology 2009;27(5):754-62.
4. Brekken RA, Sage EH. SPARC, a matricellular protein: at the crossroads of cell-matrix communication. Matrix Biol 2001;19(8):816-27.
5. Sangaletti S, Tripodo C, Vitali C, Portararo P, Guarnotta C, Casalini P, et al. Defective stromal remodeling and neutrophil extracellular traps in lymphoid tissues favor the transition from autoimmunity to lymphoma. Cancer Discov 2014;4(1):110-29.
6. Tefferi A, Vaidya R, Caramazza D, Finke C, Lasho T, Pardanani A. Circulating interleukin (IL)-8, IL-2R, IL-12, and IL-15 levels are independently prognostic in primary myelofibrosis: a comprehensive cytokine profiling study. Journal of clinical oncology : official journal of the American Society of Clinical Oncology 2011;29(10):1356-63.
7. Kornblau SM, McCue D, Singh N, Chen W, Estrov Z, Coombes KR. Recurrent expression signatures of cytokines and chemokines are present and are independently prognostic in acute myelogenous leukemia and myelodysplasia. Blood 2010;116(20):4251-61.
8. Sangaletti S, Tripodo C, Cappetti B, Casalini P, Chiodoni C, Piconese S, et al. SPARC oppositely regulates inflammation and fibrosis in bleomycin-induced lung damage. Am J Pathol 2011;179(6):3000-10.
9. Sangaletti S, Tripodo C, Chiodoni C, Guarnotta C, Cappetti B, Casalini P, et al. Neutrophil extracellular traps mediate transfer of cytoplasmic neutrophil antigens to myeloid dendritic cells toward ANCA induction and associated autoimmunity. Blood 2012;120(15):3007-18.
10. Kessenbrock K, Krumbholz M, Schonermarck U, Back W, Gross WL, Werb Z, et al. Netting neutrophils in autoimmune small-vessel vasculitis. Nat Med 2009;15(6):623-5.
11. Garcia-Romo GS, Caielli S, Vega B, Connolly J, Allantaz F, Xu Z, et al. Netting neutrophils are major inducers of type I IFN production in pediatric systemic lupus erythematosus. Science translational medicine 2011;3(73):73ra20.
12. Swerdlow SH, Campo, E., Harris, N.L., Jaffe, E.S., Pileri, S.A., Stein, H., Thiele, J., Vardiman, J.W. WHO Classification of Tumours of Haematopoietic and Lymphoid Tissues, Fourth Edition. WHO Classification of Tumours 2008;2.
13. Schauer C, Janko C, Munoz LE, Zhao Y, Kienhofer D, Frey B, et al. Aggregated neutrophil extracellular traps limit inflammation by degrading cytokines and chemokines. Nat Med 2014;20(5):511-7.
14. Kristinsson SY, Bjorkholm M, Hultcrantz M, Derolf AR, Landgren O, Goldin LR. Chronic immune stimulation might act as a trigger for the development of acute myeloid leukemia or myelodysplastic syndromes. Journal of clinical oncology : official journal of the American Society of Clinical Oncology 2011;29(21):2897-903.
15. Lande R, Ganguly D, Facchinetti V, Frasca L, Conrad C, Gregorio J, et al. Neutrophils activate plasmacytoid dendritic cells by releasing self-DNA-peptide complexes in systemic lupus erythematosus. Science translational medicine 2011;3(73):73ra19.

16. Fuchs TA, Abed U, Goosmann C, Hurwitz R, Schulze I, Wahn V, et al. Novel cell death program leads to neutrophil extracellular traps. The Journal of cell biology 2007;176(2):231-41.
17. Metzler KD, Fuchs TA, Nauseef WM, Reumaux D, Roesler J, Schulze I, et al. Myeloperoxidase is required for neutrophil extracellular trap formation: implications for innate immunity. Blood 2011;117(3):953-9.
18. Falini B, Mecucci C, Tiacci E, Alcalay M, Rosati R, Pasqualucci L, et al. Cytoplasmic nucleophosmin in acute myelogenous leukemia with a normal karyotype. N Engl J Med 2005;352(3):254-66.
19. Oostendorp RA, Audet J, Eaves CJ. High-resolution tracking of cell division suggests similar cell cycle kinetics of hematopoietic stem cells stimulated in vitro and in vivo. Blood 2000;95(3):855-62.
20. Kohlmann A, Kipps TJ, Rassenti LZ, Downing JR, Shurtleff SA, Mills KI, et al. An international standardization programme towards the application of gene expression profiling in routine leukaemia diagnostics: the Microarray Innovations in LEukemia study prephase. Br J Haematol 2008;142(5):802-7.
21. Haferlach T, Kohlmann A, Wieczorek L, Basso G, Kronnie GT, Bene MC, et al. Clinical utility of microarray-based gene expression profiling in the diagnosis and subclassification of leukemia: report from the International Microarray Innovations in Leukemia Study Group. Journal of clinical oncology : official journal of the American Society of Clinical Oncology 2010;28(15):2529-37.
22. Verhaak RG, Wouters BJ, Erpelinck CA, Abbas S, Beverloo HB, Lugthart S, et al. Prediction of molecular subtypes in acute myeloid leukemia based on gene expression profiling. Haematologica 2009;94(1):131-4.
23. de Jonge HJ, Valk PJ, Veeger NJ, ter Elst A, den Boer ML, Cloos J, et al. High VEGFC expression is associated with unique gene expression profiles and predicts adverse prognosis in pediatric and adult acute myeloid leukemia. Blood 2010;116(10):1747-54.
24. Visani G, Ferrara F, Di Raimondo F, Loscocco F, Sparaventi G, Paolini S, et al. Low-dose lenalidomide plus cytarabine induce complete remission that can be predicted by genetic profiling in elderly acute myeloid leukemia patients. Leukemia 2014;28(4):967-70.
25. Long SA, Buckner JH. CD4+FOXP3+ T regulatory cells in human autoimmunity: more than a numbers game. J Immunol 2011;187(5):2061-6.
26. Piconese S, Pittoni P, Burocchi A, Gorzanelli A, Care A, Tripodo C, et al. A non-redundant role for OX40 in the competitive fitness of Treg in response to IL-2. Eur J Immunol 2010;40(10):2902-13.
27. Martinelli S, Urosevic M, Daryadel A, Oberholzer PA, Baumann C, Fey MF, et al. Induction of genes mediating interferon-dependent extracellular trap formation during neutrophil differentiation. J Biol Chem 2004;279(42):44123-32.
28. Brinkmann V, Reichard U, Goosmann C, Fauler B, Uhlemann Y, Weiss DS, et al. Neutrophil extracellular traps kill bacteria. Science (New York, NY 2004;303(5663):1532-5.
29. Okada S, Nakauchi H, Nagayoshi K, Nishikawa S, Miura Y, Suda T. In vivo and in vitro stem cell function of c-kit- and Sca-1-positive murine hematopoietic cells. Blood 1992;80(12):3044-50.
30. Bottero V, Withoff S, Verma IM. NF-kappaB and the regulation of hematopoiesis. Cell Death Differ 2006;13(5):785-97.
31. Cheng K, Sportoletti P, Ito K, Clohessy JG, Teruya-Feldstein J, Kutok JL, et al. The cytoplasmic NPM mutant induces myeloproliferation in a transgenic mouse model. Blood 2010;115(16):3341-5.
32. Zhang L, Gajewski TF, Kline J. PD-1/PD-L1 interactions inhibit antitumor immune responses in a murine acute myeloid leukemia model. Blood 2009;114(8):1545-52.

33. Nawa Y, Kawahara K, Tancharoen S, Meng X, Sameshima H, Ito T, et al. Nucleophosmin may act as an alarmin: implications for severe sepsis. J Leukoc Biol 2009;86(3):645-53.
34. Falini B, Bolli N, Shan J, Martelli MP, Liso A, Pucciarini A, et al. Both carboxy-terminus NES motif and mutated tryptophan(s) are crucial for aberrant nuclear export of nucleophosmin leukemic mutants in NPMc+ AML. Blood 2006;107(11):4514-23.
35. Papaemmanuil E, Gerstung M, Bullinger L, Gaidzik VI, Paschka P, Roberts ND, et al. Genomic Classification and Prognosis in Acute Myeloid Leukemia. N Engl J Med 2016;374(23):2209-21.
36. Sportoletti P, Varasano E, Rossi R, Bereshchenko O, Cecchini D, Gionfriddo I, et al. The human NPM1 mutation A perturbs megakaryopoiesis in a conditional mouse model. Blood 2013;121(17):3447-58.
37. Vassiliou GS, Cooper JL, Rad R, Li J, Rice S, Uren A, et al. Mutant nucleophosmin and cooperating pathways drive leukemia initiation and progression in mice. Nat Genet 2011;43(5):470-5.
38. Falini B, Nicoletti I, Bolli N, Martelli MP, Liso A, Gorello P, et al. Translocations and mutations involving the nucleophosmin (NPM1) gene in lymphomas and leukemias. Haematologica 2007;92(4):519-32.
39. Grisendi S, Bernardi R, Rossi M, Cheng K, Khandker L, Manova K, et al. Role of nucleophosmin in embryonic development and tumorigenesis. Nature 2005;437(7055):147-53.

**Figures and legends**

**Figure 1**

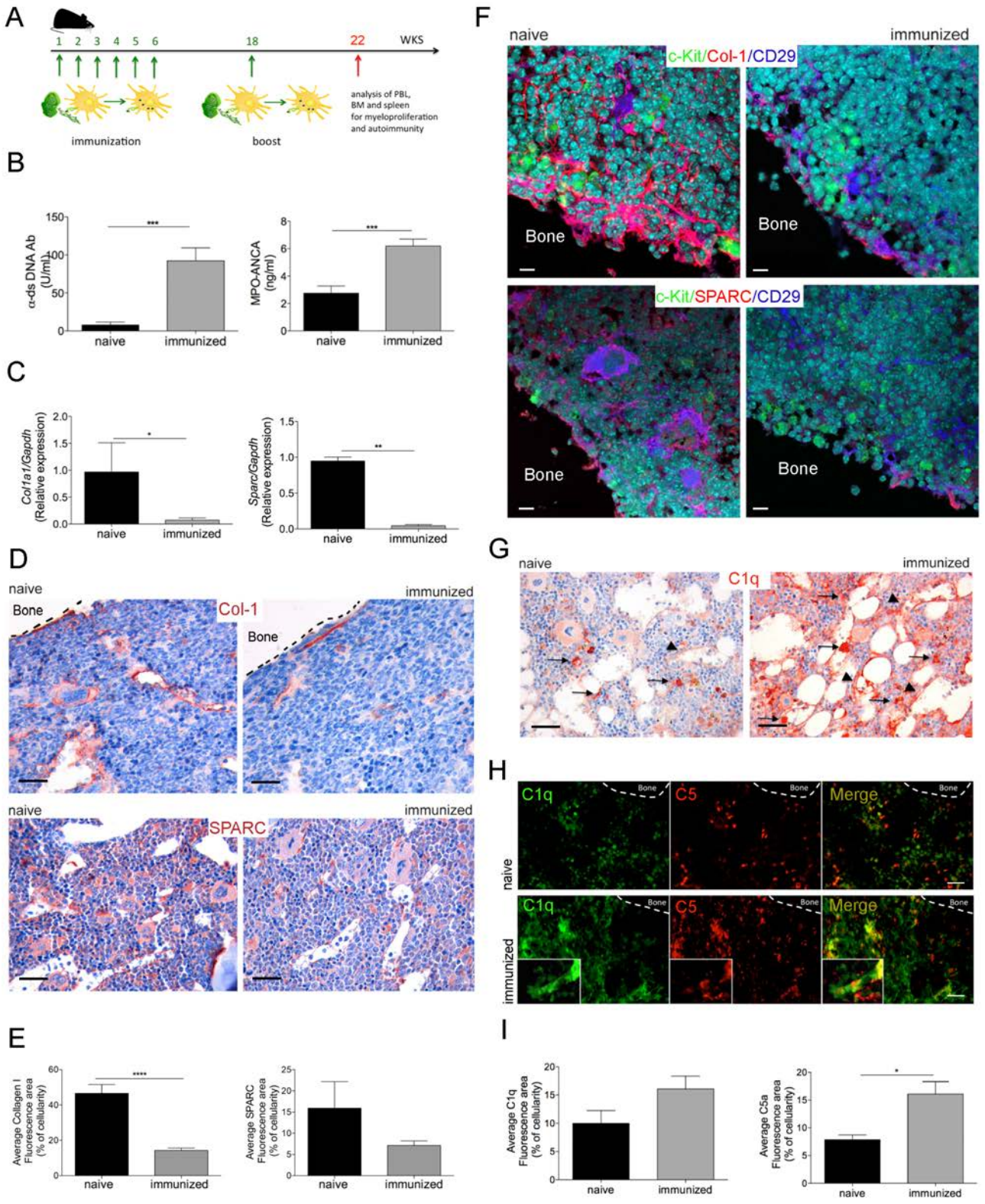


*Figure 1. Chronic immune stimulation induces stromal changes in the BM.* **A.** Schematic representation of NET-loaded DC-based immunization protocol. **B.** Quantification of anti-dsDNA autoantibodies and MPO-ANCA levels in immunized and control mice. Data are expressed as

U/mL of IgG for anti-ds DNA or as ng/ml of IgG for MPO-ANCA (n=10/each group; ***p<0.001, Mann-Whitney test). **C.** Expression of *Sparc* and *Col1a1* in total BM cells isolated from immunized and control mice. The fold change in the expression of the target genes relative to the internal control gene (GAPDH) is shown (n=5; *p<0.05, Mann-Whitney test). **D.** Representative IHC analysis of type I collagen and SPARC shows the reduction of both ECM molecules in the BM of immunized mice. Scale bars: 50 μm. **E.** Quantitative analysis of collagen type I and SPARC in IF images as detailed in Supplementary methods. **F**. Representative triple confocal microscopy analysis of type I collagen or SPARC, together with CD29 and c-Kit performed on BM sections from immunized and control mice. The image shows the reduction of type I collagen and SPARC expression in mesenchymal ($CD29^+$) cells of the osteoblastic niche that is enriched in hematopoietic (c-Kit+) hematopoietic precursors. Scale bars: 10 μm. **G.** IHC of C1q in BM sections from immunized and control mice showing an increase in vascular (arrows) and stromal (arrowheads) C1q expression in immunized mice. **H**. Representative double IF analysis showing that the increased C1q induction in the BM of immunized mice is associated with an increase in the stromal deposition of C5a. **I**. Quantitative analysis of C1q and C5a in IF images as detailed in supplementary methods.

**Figure 2**

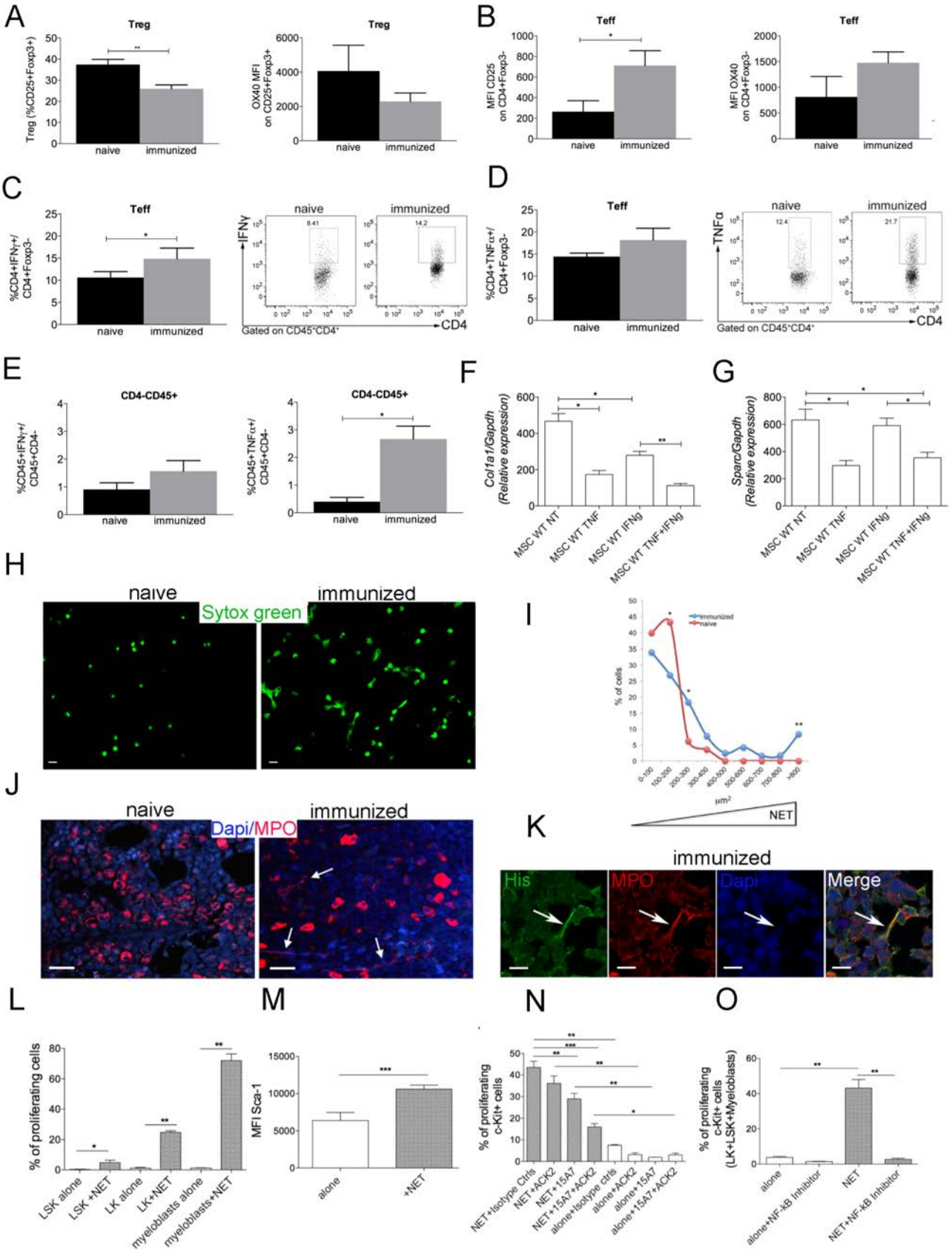


*Figure 2. A pro-inflammatory BM microenvironment supports NET formation, thereby promoting hematopoietic precursor proliferation*. **A**. Reduced frequency of $CD4^+CD25^+Foxp3^+$ Tregs and

their reduction in OX40 fitness marker expression (MFI) in BM of immunized (grey bar) compared to naïve (black bar) mice. **B.** Activation of $CD4^+Foxp3^-$ Teff upon immunization evaluated in terms of CD25 and OX40 expression. **C-D.** Activation of $CD4^+Foxp3^-$ Teff upon immunization evaluated as IFNγ and TNF secretion. The frequency of IFNγ and TNF secreting cells was evaluated within the gate of CD4+ and Foxp3- cells as shown in the relative representative gating strategy. **E** IFNγ and TNF secretion by non-CD4 leukocytes in the BM of naive (black bar) and vaccinated (grey bar) mice. Data are representative of three independent experiments, each including 5 mice per groups; statistical analysis: student's T-test: *p<0.05; **p<0.01. **F-G.** Expression of *Col1a* and *Sparc* genes in BM-MSC stimulated or not with IFNγ, TNF or their combination. The fold change in expression of the target genes relative to the internal control gene (GAPDH) is shown. Scale bars: 10 μm. **H.** *Ex vivo* spontaneous NET formation by PMNs isolated from the BM of immunized or control mice. Spontaneous NET formation was evaluated by seeding BM-isolated PMNs into poly-D-lysine coated glasses in presence of the DNA-dye Sytox green. **I.** Quantification of NET formed by BM-PMNs isolated from immunized mice. Nuclear area of BM PMN from naïve and immunized mice is plotted against the percentage of SYTOX-positive cells corresponding to a given nuclear area. PMN undergoing NETosis are characterized by broad range of nuclear areas, whereas apoptotic neutrophils show smaller nuclear areas. Quantification shows that PMN from immunized mice make more NET in comparison to PMN from naïve mice. Experiments comparing the two types of BM PMN were repeated 3 times with PMN from at least 3 donor mice each. Number of nuclei analyzed/experiment= 100. **J.** IF for MPO performed on BM sections from immunized and naïve mice showing the presence of extracellular MPO threads, which is associated with NET formation (indicated by arrows), in BM sections from immunized mice. In naïve mice, MPO staining was confined to the cytoplasmic area of myeloid cells. Scale bars: 50 μm. **K.** Representative confocal microscopy analysis showing the co-localization of citrullinated histone H3, MPO and Dapi in extracellular traps of BM from immunized mice. Scale bars: 10 μm. **L.** To determine the role of NET in hematopoietic precursor proliferation, FACS-sorted c-kit+ BM cells were stained with the proliferation dye CFSE and co-cultured with NET. The proliferative effect of NETs was analyzed in the different fractions of $c\text{-}Kit^+$ hematopoietic cells (see Supplementary Figure 2B for representative plots)(n = 10 per group; **p < 0.01, Mann-Whitney test). **M.** Expression of Sca (MFI) in $c\text{-}Kit^+Sca^+GR\text{-}1^-$ early progenitors co-cultured or not with NET (n = 10 per group; **p < 0.01, Mann-Whitney test). **N.** Proliferation of CFSE-labeled FACS-sorted $Lin^-c\text{-}Kit^+$ cells to NETs in presence of mAbs blocking SCF-1 (ACK2) or IL-6 (15A7) or isotype controls (n = 10 per group, excluding controls. For controls n = 5 per group; ***p < 0.001, **p < 0.01; * p < 0.05; Mann-Whitney test).

**O.** Inhibition of NET-induced $Lin^{-}c\text{-}Kit^{+}$ cell proliferation by a specific NF-kB inhibitor (InSolution NF-kB activation inhibitor, Calbiochem) (n = 6 per group; **p < 0.01, Mann-Whitney test). NF-kB inhibition completely abrogated the NET-induced proliferation of $c\text{-}Kit^{+}$ cells.

**Figure 3**

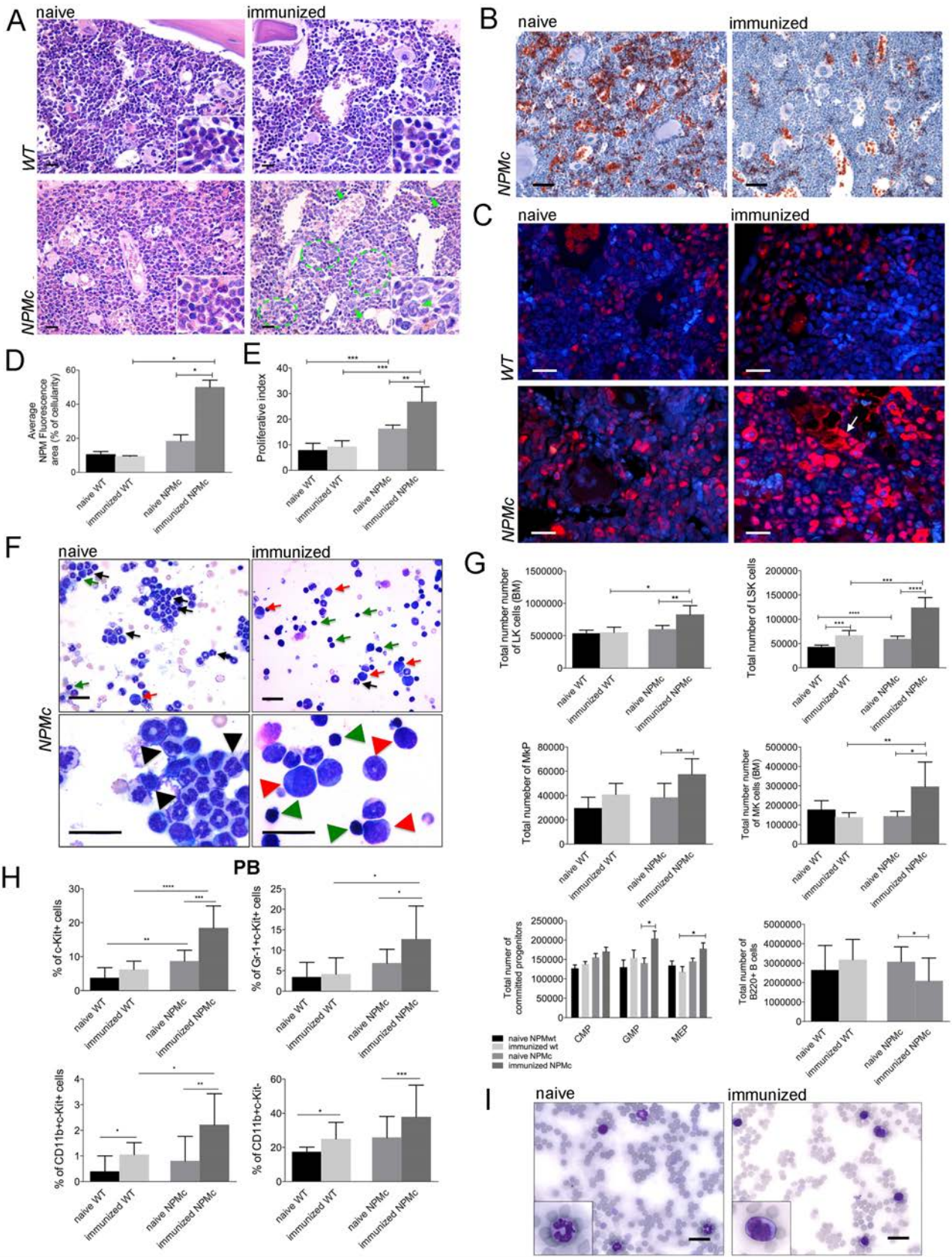
A
naive
immunized
WT
NPMc
B
naive
immunized
NPMc
C
naive
immunized
WT
NPMc
D
Average NPM Fluorescence area (% of cellularity)
naive WT
immunized WT
naive NPMc
immunized NPMc
E
Proliferative index
F
naive
immunized
NPMc
G
Total number number of LK cells (BM)
Total number of LSK cells
Total numeber of MkP
Total number number of MK cells (BM)
Total numer of committed progenitors
CMP
GMP
MEP
naive NPMwt
immunized wt
naive NPMc
immunized NPMc
Total number of B220+ B cells
H
PB
% of c-Kit+ cells
% of Gr-1+c-Kit+ cells
% of CD11b+c-Kit+ cells
% of CD11b+c-Kit-
I
naive
immunized

*Figure 3. NET-associated immune stimulation cooperates the with NPMc background in shaping the myeloproliferative phenotype*. **A.** Representative BM histopathology showing hematopoietic parenchyma of WT and *NPMc* naïve and immunized mice. *NPMc* transgenic mice exhibit myeloproliferative features with prominent mature granulocytopoiesis. Upon immunization, the exacerbated myelopoiesis of *NPMc* mice becomes dysplastic with significant left-shift of myel- and megakaryocytopoiesis and increase in atypical myeloid precursor clusters (arrowheads, inset). Signs of intravascular hematopoiesis are evident in these samples (dashed green line). Scale bars: 50 μm. **B**. IHC analysis for the erythroid Ter119 marker on BM paraffin sections from immunized and naive *NPMc* mice. Scale bars: 100 μm**. C.** Representative IF analysis for NPM performed on BM paraffin sections from naïve or immunized WT and *NPMc* mice. Scale bars: 50 μm. **D.** Quantitative analysis of NPM immunofluorescence performed on 5 BM sections from naïve and immunized *NPMc* or WT mice; Statistical analysis: Student *t* test; *p<0.05. **E.** Quantification of the Ki-67 proliferative index in BM biopsies from immunized and naive *NPMc* or WT mice. (n=5 per group; Statistical analysis: Student *t* test; **p<0.01;***p<0.001). **F.** BM smears of immunized *NPMc* mice showed an increase in myeloid blasts with atypical morphology (red arrows), a concomitant decrease in segmented mature granulocytes (black arrows), and an increase in lymphoid elements (green arrows) compared with naive *NPMc* mice, which showed a predominance of segmented granulocytes and rare blasts. Scale bars: 20 μm. **G.** BM FACS analyses showing the total amount of $Lin^{-}$c-$Kit^{+}$ and $Lin^{-}Sca1^{+}Kit^{+}$ precursor cells and myeloid progenitors (GMP) in the BM of immunized *NPMc* mice. The induction of megakaryocytes (Mk) and their progenitors (MkP) was also observed. (n=10 per group; Statistical analysis: Student *t* test; *p<0.05;**p<0.01;***p<0.001). The exacerbated myelopoiesis of immunized *NPMc* mice was associated with a slight but significant decrease in $B220^{+}$ lymphoid cells. **H**. PB FACS analysis showing the increased percentage of the overall circulating c-$Kit^{+}$ cells, myeloblasts (Gr-$1^{+}$c-$Kit^{+}$ and $CD11b^{+}$c-$Kit^{+}$), and mature $CD11b^{+}$ myeloid cells, in immunized *NPMc* transgenic mice. **I.** Representative PB smears from naïve and immunized *NPMc* mice showing the presence of circulating atypical immature myeloid cells in the PB of immunized but not naïve transgenic mice. Scale bars: 20 μm.

**Figure 4**

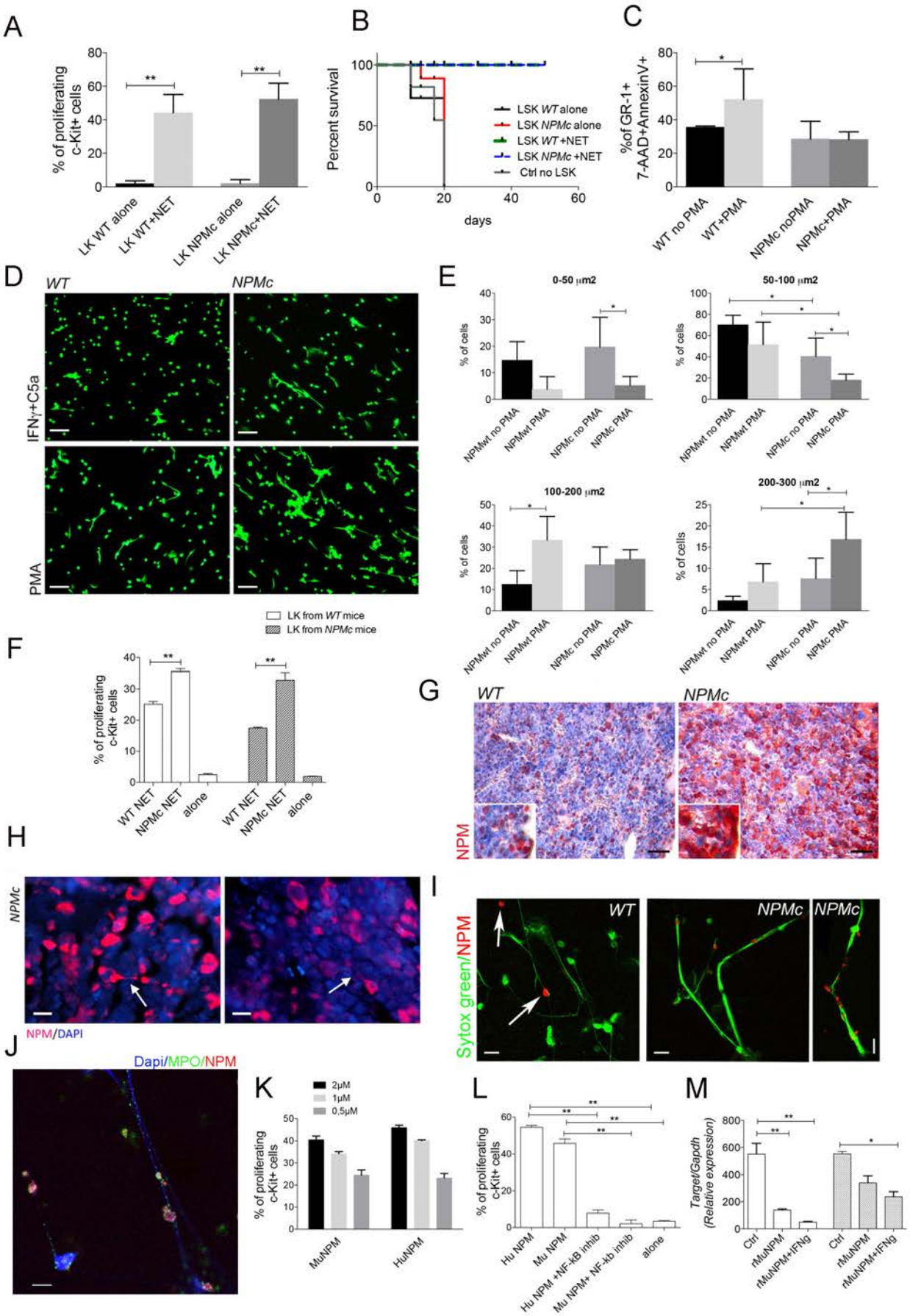
A
% of proliferating c-Kit+ cells
LK WT alone
LK WT+NET
LK NPMc alone
LK NPMc+NET
B
Percent survival
days
LSK WT alone
LSK NPMc alone
LSK WT +NET
LSK NPMc +NET
Ctrl no LSK
C
%of GR-1+ 7-AAD+AnnexinV+
WT no PMA
WT+PMA
NPMc noPMA
NPMc+PMA
D
WT
NPMc
IFNγ+C5a
PMA
LK from WT mice
LK from NPMc mice
E
0-50 μm2
50-100 μm2
100-200 μm2
200-300 μm2
% of cells
NPMwt no PMA
NPMwt PMA
NPMc no PMA
NPMc PMA
F
% of proliferating c-Kit+ cells
WT NET
NPMc NET
alone
G
WT
NPMc
NPM
H
NPMc
NPM/DAPI
I
WT
NPMc
NPMc
Sytox green/NPM
J
Dapi/MPO/NPM
K
2μM
1μM
0,5μM
% of proliferating c-Kit+ cells
MuNPM
HuNPM
L
% of proliferating c-Kit+ cells
Hu NPM
Mu NPM
Hu NPM +NF-kB inhib
Mu NPM+ NF-kb inhib
alone
M
Target/Gapdh (Relative expression)
Ctrl
rMuNPM
rMuNPM+IFNg

*Figure 4. NPMc mutation increases the proliferative response of hematopoietic precursors to NET stimulation*. **A.** FACS-sorted $Lin^-c\text{-}Kit^+$ cells were isolated from *NPMc* and WT mice, co-cultured with NETs and evaluated for proliferation *in vitro*. The panel shows that the *NPMc* mutation does not confer a cell-intrinsic proliferative advantage to $c\text{-}Kit^+$ cells as the proliferative response to NET is comparable in the two genotypes. **B.** $Lin^-Sca1^+Kit^+$ cells from *NPMc* and WT mice were co-cultured in the presence or absence of NET, without other supplements, and injected intravenously into lethally irradiated WT mice. All the mice receiving $Lin^-Sca1^+Kit^+$ co-cultured with NETs survived independently from the *NPMc* genotype of the transplanted cells. **C.** Neutrophils were isolated from the BM of *NPMc* and WT mice and treated with PMA for 24 h. Upon PMA-mediated activation, *NPMwt* and *NPMc* PMNs exhibited a different rate of apoptosis, which was higher in the former group. **D.** Increased NET formation by *NPMc* mutant neutrophils compared with their *NPMwt* counterparts in response to IFNγ+C5a or PMA activation (quantification is showed in Supplementary Figure 10). Scale bars: 20 μm. **E.** Quantification of NET formation is showed for PMA-treated *NPMc* and WT neutrophils. Nuclear areas are plotted against the percentage of SYTOX- positive cells corresponding to a given nuclear area. PMN showing an enhanced propensity to undergo NETosis display an increased frequency of nuclei with highest nuclear areas. In this experiment the SYTOX green DNA dye was added to PMN after PFA-fixation, 18h later. Experiments comparing PMN from *NPMc* transgenic or *WT* mice were repeated 3 times with PMN from at least 3 donor mice each. Number of nuclei analyzed/experiment= 200. (* $p< 0{,}05$, Mann-Whitney t test). **F.** FACS-sorted $Lin^-c\text{-}Kit^+$ cells were isolated from the BM of *NPMc* and *NPMwt* mice and co-cultured with NETs obtained from *NPMc* and *NPMw*t mice. The image shows that *NPMc*-derived NETs promoted the proliferation of $c\text{-}Kit^+$ hematopoietic cells more efficiently in a 48 h (instead of 72h) assay. **G.** IHC for NPM was performed on BM sections from *NPMc* and *NPMwt* mice. The representative image shows that, in *NPMc* transgenic mice, cytoplasmic staining of NPM revealed hematopoietic myeloid cells, including mature granulocytes, scattered throughout the BM interstitium. This was not observed in the BM of the *NPMwt* mice. Scale bars: 50 μm. **H.** IF analysis of the BM of *NPMc* mice showing that NPM is detected in association with MP0+ DNA-thread structures suggestive of NET (indicated via arrows). Scale bars: 20 μm. **I.** Confocal IF analysis for NPM performed in BM neutrophils from *NPMwt* and *NPMc* mice seeded onto poly-D-Lysine coated glasses and stimulated with PMA to induce NET formation. Staining for NPM (red signal) was performed without permeabilizing cells, which allowed detection of only NPM associated with extruded NET (highlighted by the DNA dye Sytox green, green signal) in *NPMc* neutrophils or apoptotic cells (arrow) in NPMwt neutrophils, but not NPM retained within live cells.

In *NPMwt* neutrophils, NPM was not detected, except in apoptotic cells (indicated by arrows). Scale bars: 10 μm. **J.** Confocal microscopy analysis performed on NET from *NPMc* neutrophils showing NPM colocalizing with MPO, a classical NET-associated proteins, onto the DNA (Dapi staining) threads. Scale bars: 10 μm. **K-L.** Proliferation of CFSE-labeled FACS-sorted $Lin^{-}c\text{-}Kit^{+}$ cells in response to recombinant murine and human NPM, with or without NF-kB inhibitor. Proliferation was evaluated at 72 h (n = 5/group; $^{**}p < 0.01$, Mann-Whitney test). **M.** Expression of *Col1a* and *Sparc* genes in BM-MSC stimulated or not with IFNγ, TNF or their combination. The fold change in expression of the target genes relative to the internal control gene (GAPDH) is shown.

**Figure 5**

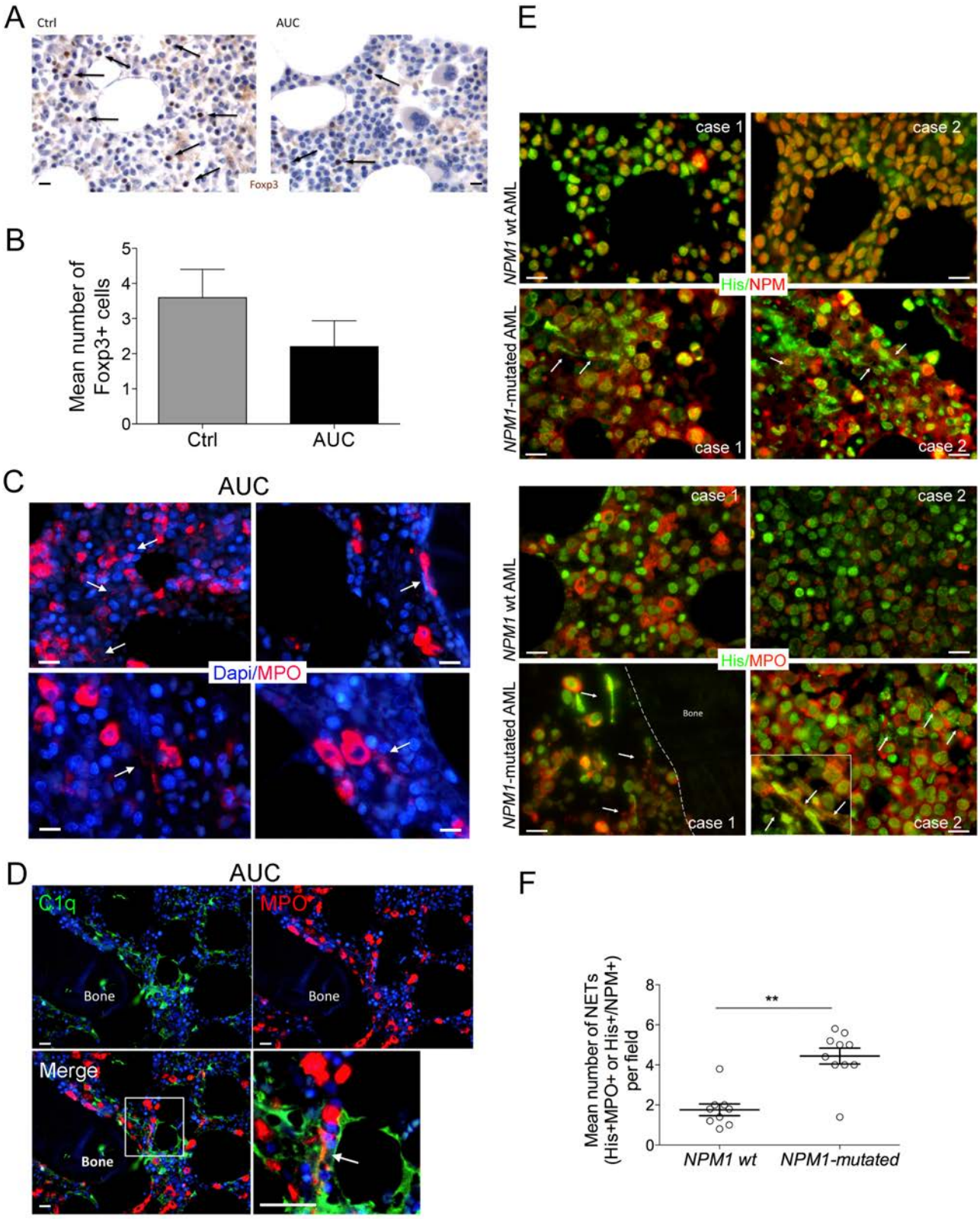


*Figure 5. In situ NET detection in autoimmune and NPM1-mutated AML patients*. **A.** IHC analysis for Foxp3 performed on one representative case of autoimmune patient compared to healthy control. Foxp3+ Treg are highlighted through arrows. Scale bars: 20 μm. **B.** Mean number of Foxp3+ cells

in the BM of autoimmune patients (cumulative data; n=5/fields/patient; n=12/group patients). Scale bars: 20 μm. **C**. IF for MPO of BM sections from patients with autoimmunity-associated cytopenias (patients #4 and #9, Supplementary Table 1) showing the presence of extracellular MPO threads suggestive of NET formation within the BM interstitium. **D.** Representative IF analysis of BM from a patient with autoimmunity-associated cytopenia (patient #4, Supplementary Table 1) showing C1q complement deposition in BM stromal cells and the close proximity between C1q+ stromal elements (green) and NET MPO threads (red) (arrow). Scale bars: 20 μm. **E.** Representative double-marker immunofluorescence microphotographs of WT and NPM1 mutated human AML BM biopsies showing the presence of histone H3 threads (green signal) associated with either NPM (red signal, upper panels) or MPO (red signal, lower panels) in NET structures (arrows). NET histone H3 threads were prevalently detected in NPM1 mutated cases, in which NPM was relocalized into the cytoplasm. Scale bars: 20 μm. **F.** Mean number of NETs, evaluated as MPO+ or NPM+ histone H3+ double positive threads, in BM biopsies from WT and NPM1 mutated AML (for patients details: Supplementary Table 7).

## Figure 6

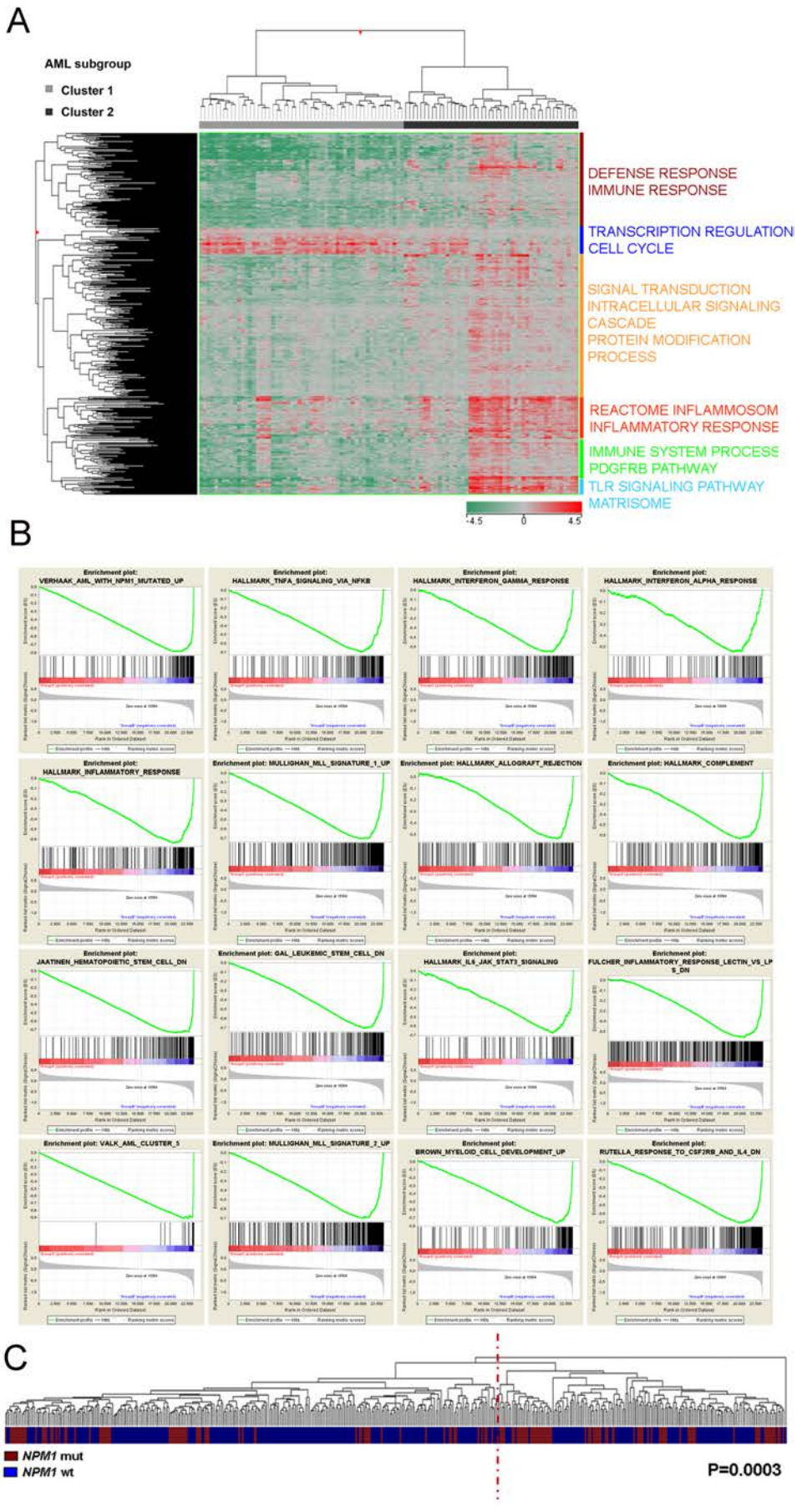
A
AML subgroup
Cluster 1
Cluster 2
DEFENSE RESPONSE
IMMUNE RESPONSE
TRANSCRIPTION REGULATION
CELL CYCLE
SIGNAL TRANSDUCTION
INTRACELLULAR SIGNALING CASCADE
PROTEIN MODIFICATION PROCESS
REACTOME INFLAMMOSOM
INFLAMMATORY RESPONSE
IMMUNE SYSTEM PROCESS
PDGFRB PATHWAY
TLR SIGNALING PATHWAY
MATRISOME
-4.5
0
4.5
B
Enrichment plot: VERHAAK_AML_WITH_NPM1_MUTATED_UP
Enrichment plot: HALLMARK_TNFA_SIGNALING_VIA_NFKB
Enrichment plot: HALLMARK_INTERFERON_GAMMA_RESPONSE
Enrichment plot: HALLMARK_INTERFERON_ALPHA_RESPONSE
Enrichment plot: HALLMARK_INFLAMMATORY_RESPONSE
Enrichment plot: MULLIGHAN_MLL_SIGNATURE_1_UP
Enrichment plot: HALLMARK_ALLOGRAFT_REJECTION
Enrichment plot: HALLMARK_COMPLEMENT
Enrichment plot: JAATINEN_HEMATOPOIETIC_STEM_CELL_DN
Enrichment plot: GAL_LEUKEMIC_STEM_CELL_DN
Enrichment plot: HALLMARK_IL6_JAK_STAT3_SIGNALING
Enrichment plot: FULCHER_INFLAMMATORY_RESPONSE_LECTIN_VS_LPS_DN
Enrichment plot: VALK_AML_CLUSTER_5
Enrichment plot: MULLIGHAN_MLL_SIGNATURE_2_UP
Enrichment plot: BROWN_MYELOID_CELL_DEVELOPMENT_UP
Enrichment plot: RUTELLA_RESPONSE_TO_CSF2RB_AND_IL4_DN
C
NPM1 mut
NPM1 wt
P=0.0003

*Figure 6. A NET-related inflammatory gene signature subdivides acute myeloid leukemias*

**A.** Supervised analysis of AML cases divided by cluster (1 vs. 2) as defined by the expression of the NET-related inflammatory signature. The two clusters differ in the expression of 440 genes belonging to programs of inflammation, immune response, leukemic stemness, and, notably NPM-1 signaling. In the matrix, each column represents a sample and each row represents a gene. The color scale bar shows the relative gene expression changes normalized to the standard deviation (0 is the mean expression level of a given gene). The main Biological Processes (GeneOntology) identified by gene set enrichment analysis are highlighted on the right. **B.** GSEA of the differentially expressed genes in AML cluster 1 *vs*. AML cluster 2 showing the positive enrichment of diverse inflammatory programs in AML cluster 2. The enrichment score relative to the different datasets is shown. **C.** Hierarchical clustering of AML cases based on the NET-related inflammatory signature showing that *NMP1* mutated cases were significantly segregated (chi-square, $p < 0.001$) according to the signature.

**Figure 7**

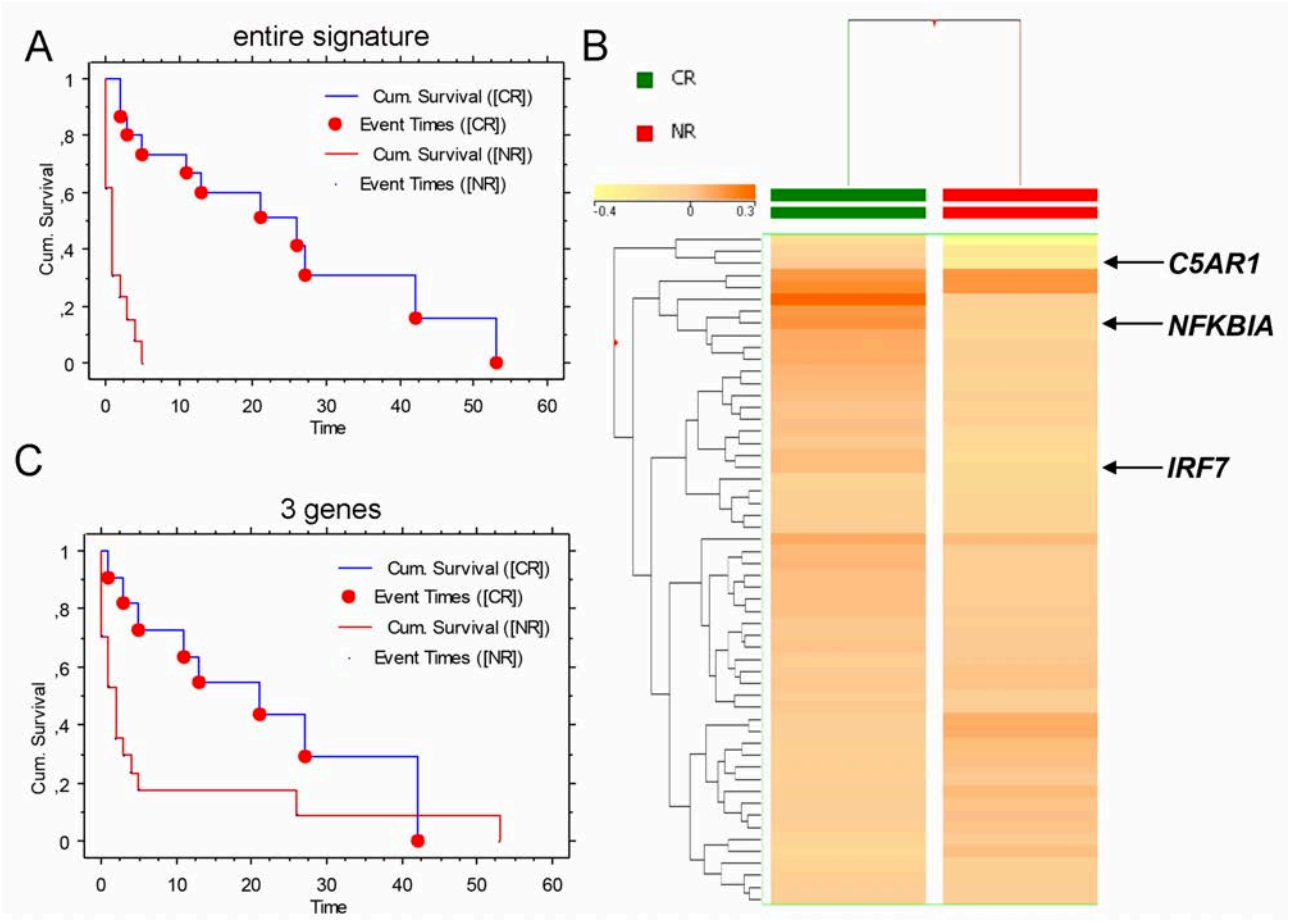


*Figure 7. The NET-related inflammatory gene signature predicts response to immunomodulatory drugs*. **A.** Overall survival curves (Kaplan Meier method) of AML patients treated with lenalidomide plus AraC classified into two groups (group 1, responders, blue line; group 2, non responders, red line) based on the expression of the entire NET-related inflammatory signature (Support vector machine algorithm). **B**. Three genes belonging to the NET-related inflammatory signature were found among those differentially expressed according to the clinical response (CR vs. no CR achievement) in AML patients receiving lenalidomide plus AraC (24). **C.** Overall survival curves (Kaplan Meier method) of AML patients treated with lenalidomide plus AraC classified into two groups (group 1, responders, blue line; group 2, non responders, red line) based on the three genes of the NET-related inflammatory signature (*C5AR1*, *NFKBIA*, *IRF7*) (Support vector machine algorithm).